ChemComm

Accepted Manuscript

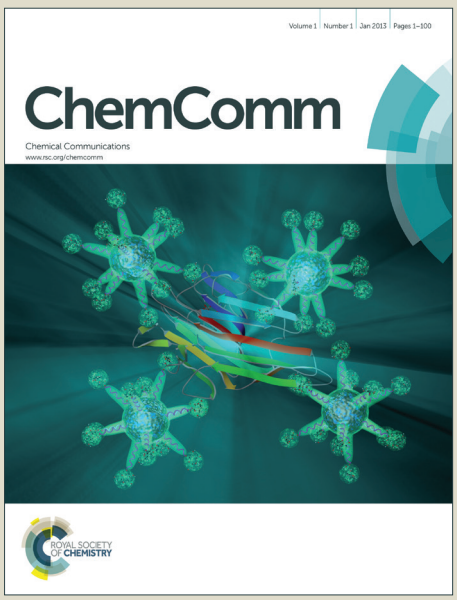

ROYAL SOCIETY OF CHEMISTRY

www.rsc.org/chemcomm

Journal Name

RSCPublishing

COMMUNICATION

MoS_2 nanosheet/TiO_2 nanowire hybrid nanostructures for enhanced visible-light photocatalytic activities

Cite this: DOI: 10.1039/xoxxoooooox

Meng Shen,[a] Zhiping Yan,[a] Lei Yang,[a] Pingwu Du,*[a] Jingyu Zhang,[b] Bin Xiang*[a]

Received ooth January 2012,
Accepted ooth January 2012

DOI: 10.1039/xoxxoooooox

www.rsc.org/

Molybdenum disulfide (MoS_2) with a layered structure has attracted much attention on photocatalytic water splitting for hydrogen production owing to its chemical stability. However, the inherent stacking property screens part of MoS_2 active sites which retards catalytic reactions. Herein, we report one dimensional (1D) MoS_2 nanosheet/porous TiO_2 nanowire (shell/core) hybrid nanostructures synthesized by a simple hydrothermal method, leading to an enhanced specific surface area (66 m^2/g) compared to MoS_2 nanosheets (48 m^2/g). Scanning Electron Microscope (SEM), Transmission Electron Microscope (TEM), X-ray Diffraction (XRD) and Raman spectrum were utilized to confirm the 1D MoS_2/TiO_2 hybrid nanostructures. This 1D hybrid nanostructures with a porous core as co-catalyst exhibit high activity in visible light photocatalytic hydrogen evolution reaction (HER) with an enhanced hydrogen generation rate of 16.7 $mmol \cdot h^{-1} \cdot g^{-1}$. Our results provide some general guidelines in the search for enhancing visible-light photocatalytic HER.

Due to its excellent electronic and optical properties, MoS_2, a transitional metal dichalcogenides semiconductor with a layered structure, has attracted much attention on catalysis,[1] lithium ion battery,[2] micro-electronics[3] and optoelectronic devices.[4,5] Layered MoS_2 is composed of a two-dimensional (2D) structure which includes an atomic layer of Mo atoms sandwiched between two layers of S atoms. It has been revealed that with the thickness of MoS_2 decreasing to monolayer, there is a transformation observed from indirect band gap (1.3 eV) to direct band gap (1.8 eV).[4,6,7] Recently, more studies have focused on the photocatalytic property of MoS_2 because of its special chemical stability in reactions.[8-12] Both high-resolution scanning tunneling microscopy (STM) and theoretical calculations have proved that active sites of layered MoS_2 are on the undercoordinated sulfur edges.[13-15] However, the layered configuration with low specific surface area can cause inefficient reactant molecular adsorption. In addition, stacking character can block the active sites on 2D nanosheets and cause inefficient carrier transfer, which dramatically reduces the catalytic activities. Efforts have been made to overcome these limitations. For instance, MoS_2 nanosheet/graphene hybrid structure has been employed to enhance the specific surface area of MoS_2 nanosheets, resulting in a high performance of photocatalytic HER from water splitting with a hydrogen generation rate of 165.3 μmol • h^{-1} (2.1mmol • h^{-1} • g^{-1}) under UV light irradiation.[16] In the presence of Eosin Y (EY) dye, MoS_2 nanosheet/reducesd graphene oxide (RGO) heterostructure was also employed to act as catalyst for a HER under visible light irradiation ($\lambda \geqslant 420$nm). The enhanced hydrogen evolution rate was 88.5mmol/h (4.4μmol • h^{-1} • g^{-1}) in 80 mL of 15% (v/v) TEOA aqueous solution (pH=9) with 20mg as prepared catalyst and 4×10^{-4} M EY.[17] TiO_2 nanobelt has been utilized to form MoS_2 nanosheet/TiO_2 nanobelt hybrid structure. The enhanced specific surface area has been attained to be 44.9 m^2/g.[18] As catalyst, it has improved the hydrogen production rate as high as 1.6mmol·h^{-1}·g^{-1}.[18] Herein, we report 1D MoS_2 nanosheet/porous TiO_2 nanowire (shell/core) hybrid nanostructures with an enhanced surface area of 66 m^2/g by a simple hydrothermal method. SEM, TEM, XRD and Raman spectrum were utilized to characterize the MoS_2/TiO_2 hybrid nanostructure. The enhanced specific surface area was measured by American Micromeritics Instrument Corporation TriStar II 3020M system. This hybrid configuration was employed as photo co-catalyst for visible light photocatalytic hydrogen generation reaction. The improved hydrogen generation rate is reached to be 16.7 $mmol \cdot h^{-1} \cdot g^{-1}$.

Figure 1a presents the morphology of pure TiO_2 nanowires with a diameter of 50-70 nm prepared by an electrospinning method.[19] The inset shows the porous morphology of pure TiO_2 nanowires, composed of interconnected TiO_2 nanoparticles with an average grain size of 8-12nm. Figure 1b shows the SEM image of the as-synthesized MoS_2 nanosheet/TiO_2 nanowire hybrid nanostructures. The low magnification TEM image shown in the inset of Figure 1b reveals that the TiO_2 nanowires were coated by few-layer MoS_2 nanosheets, forming TiO_2/MoS_2 core-shell structure. XRD patterns (Figure 1c) indicate that the as-synthesized hybrid nanostructures with well-defined crystalline consist of hexagonal phase MoS_2 and anatase phase TiO_2. Figure 1d shows high-resolution TEM image of MoS_2 nanosheet/TiO_2 nanowire hybrid structure. It indicates that most of the shells in the hybrid core/shell nanostructures consist of 5-7 layers of MoS_2 nanosheets. The lattice fringes of TiO_2

nanoparticles with a lattice spacing of 3.6Å correspond to the (101) plane. The well-defined crystalline structure of MoS_2 nanosheets are also illustrated by the lattice fringes with a lattice spacing of 6.2Å, corresponding to the plane of (002).

To further explore the property of the hybrid nanostructure, the phonon spectra of the MoS_2 nanosheet/TiO_2 nanowire were measured by Raman scattering (Figure 2a). The phonon vibrational modes of pure TiO_2 nanowies at 148 cm^{-1}, 397 cm^{-1}, 518 cm^{-1} and 638cm^{-1} correspond to the $\mathbf{E_g^1}$, $\mathbf{B_{1g}^1}$, $\mathbf{A_{1g}+B_{1g}^2}$ and $\mathbf{E_g^2}$ modes of anatase TiO_2, respectively. The Raman scattering peaks of pure MoS_2 nanosheets observed at 384 cm^{-1}, 408 cm^{-1} and 452 cm^{-1} can be assigned to the representative modes of $\mathbf{E_{2g}^1}$, A_{1g} and $\mathbf{E_{1u}^2}$, respectively. In the Raman spectrum of the MoS_2 nanosheet/TiO_2 nanowire hybrid nanostructures, there is a blue shift observed in the mode of $\mathbf{E_g^1}$ with a size of ~ 5 cm^{-1}, compared to pure TiO_2 nanowires. The blue shift is mostly due to a surface strain induced by the coated MoS_2 nanosheet on the TiO_2 surface.[20] In the meanwhile, there is also a surface strain generated in the coated MoS_2 nanosheets. It explains the observed red shifts in the modes of $\mathbf{E_{2g}^1}$ and A_{1g} with sizes of ~ 6 and 7 cm^{-1}, respectively, compared to pure MoS_2 nanosheets. The shell configuration of MoS_2 nanosheets leads to a tensile strain along the [001] and a compressive strain in the basal plane. This tensile strain along [001] direction reduces the Van der Waals force between neighboring layers, which causes a decrease in restoring force. Therefore, we observed a decrease in both of the $\mathbf{E_{2g}^1}$ and A_{1g} vibrational frequencies.[21] In terms of crystal structure, the phonon spectra of the hybrid structures confirm a core/shell configuration in our synthesized MoS_2 nanosheets/TiO_2 nanowires samples.

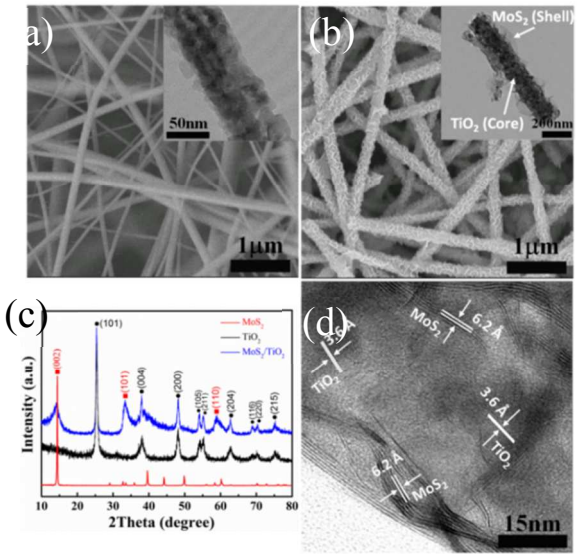

Fig. 1 (a) SEM image of pure TiO_2 nanowires. The inset shows the porous morphology of pure TiO_2 nanowires. (b) SEM image of as-synthesized MoS_2 nanosheet/TiO_2 nanowire hybrid structures. The inset is the corresponding low magnification TEM image, which presents the core/shell TiO_2 nanowire/MoS_2 nanosheet configuration. (c) XRD patterns of pure TiO_2 nanowires (black), pure MoS_2 nanosheets (red) and MoS_2/TiO_2 hybrid structures (blue). (d) High-resolution TEM image of as-synthesized MoS_2/TiO_2 hybrid structures. It exhibits the well-defined crystalline structures of the hybrid configuration.

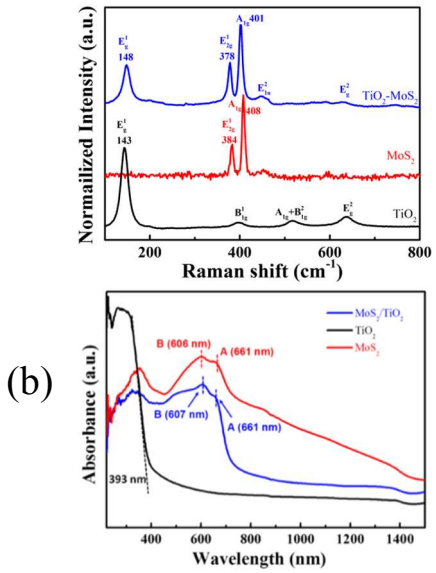

Fig. 2 (a) Raman spectra and (b) absorption spectra of pure TiO_2 nanowires (black), pure MoS_2 nanosheets (red) and as-synthesized MoS_2 nanosheet/TiO_2 nanowire hybrid structures (blue)

Figure 2b presents the absorption spectra of pure TiO_2 nanowires, pure MoS_2 nanosheets and as-synthesized MoS_2 nanosheet/TiO_2 nanowire hybrid structures. A sharp absorption edge is observed at 393 nm (3.16 eV) in the absorption spectrum of pure TiO_2 nanowires, which indicates a direct band gap of 3.16 eV in pure TiO_2 nanowires. In the absorption spectrum of pure MoS_2 nanosheets, two absorption peaks observed at 606 and 661 nm are assigned to excitonic transitions at the K point of the Brillouin zone.[22] The energy separation of ~ 0.17 eV between the two peaks is due to the spin-orbit splitting at the top of the valence band at K point.[22] Due to indirect band gap property, the absorption edge of MoS_2 nanosheets exhibits a gradual increase instead of abrupt slope. Another peak feature is observed at ~ 350 nm, which correlates to a c-axis polarized transition.[23] We also observed two representative excitonic transition peaks at ~ 607 and 661 nm in the absorption spectrum of MoS_2 nanosheet/TiO_2 nanowire hybrid structures. At the short wavelength side of the excitonic transition peaks, there is an absorption peak observed at ~ 340 nm. Since the absorption edge location of pure TiO_2 nanowires is close to the c-axis polarized transition in MoS_2 nanosheets, this peak feature at ~ 340 nm could be admixture of MoS_2 and TiO_2 absorption peaks.

To probe the photocatalytic performance, as-synthesized MoS_2 nanosheet/TiO_2 nanowire hybrid nanostructures were utilized as photo co-catalyst for visible light (λ > 420 nm) photocatalytic hydrogen generation from water splitting (details in Supporting Information). Figure 3 shows a promising hydrogen evolution rate of 16.7 $mmol \cdot h^{-1} \cdot g^{-1}$ achieved from as-synthesized MoS_2 nanosheet/TiO_2 nanowire hybrid structures photosensitized by Eosin Y under visible light illumination. In addition, the stable performance is another important requirement for co-catalyst in hydrogen evolution reactions. The inset of Figure 3 shows a good stability of photocatalytic HER catalyzed by as-synthesized MoS_2 nanosheet/TiO_2 nanowire hybrid nanostructures, which exhibits a slight saturation after 12 hours visible light illumination.

As shown in Figure 1d, the pure TiO_2 nanowires are composed of interconnected TiO_2 nanoparticles with a diameter of 8-12 nm. And we also observed numbers of pores in the TiO_2 nanowires in Figure 1d, due to the volume loss and gas release during synthesis induced from a non-equilibrium calcination process at 500℃ in air after the electrospinning step.[19] At the calcination stage, a thermal decomposition of the TiO_2 precursor triggers the nucleation and

growth of TiO_2 nanoparticles, in the meanwhile small voids are created at the nanoparticle interface due to gas release from the reactions between the carbon, nitrogen, hydrogen atoms and atmospheric oxygen. This 1D porous structure composed of quantum size TiO_2 nanoparticles provides a chance to enhance the specific surface area of MoS_2 2D nanosheets. Most of interlayer edges (acting as active sites) are covered by the outmost layers in as-synthesized multilayered pure MoS_2 nanosheets (Figure S2), which hinders the interlayer edges exposed to the reactants in hydrogen generation reactions. With an introduction of 1D TiO_2 nanowires, the 2D configuration of pure MoS_2 nanosheets was transformed into 1D structure by the formation of the MoS_2/TiO_2 hybrid nanostructures. Only several layers of MoS_2 coated, this 1D hybrid core/shell configuration provides more chances to expose the edges of MoS_2 nanosheets to the reactants in hydrogen generation reactions. The specific surface area of the hybrid nanostructures was dramatically enhanced to be ~ 66 m^2/g compared to pure MoS_2 nanosheets ($48m^2/g$). The porous morphology of the core TiO_2 nanowires also provides higher possibility to adsorb more reactant molecules into the hybrid core/shell structures. As a result, as-synthesized MoS_2 nanosheets/TiO_2 nanowires nanostructures exhibit highly reactive in the visible-light photocatalytic hydrogen evolution reaction with an enhanced hydrogen evolution rate of 16.7 mmol • h^{-1} • g^{-1}. However, using our TiO_2/MoS_2 core/shell hybrid structure as photo co-catalyst without a photosensitizer involved in for a HER, there is no hydrogen gas generation observed as shown in Figure 3. It could be due to less sufficient electron transfer in HER, resulting from weak alkalinity in TEOA. Therefore no hydrogen generation could be detected from this reaction without a photosensitizer.

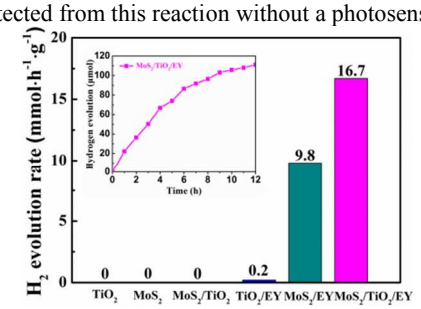

Fig. 3 Different photocatalytic hydrogen evolution rate within 3 hours under visible light illumination catalyzed by different photocatalytic systems (details in Supporting Information). The highest hydrogen evolution rate (~ 16.7 mmol • h^{-1} • g^{-1}) is achieved in the 1D MoS_2 nanosheet/TiO_2 nanowire hybrid nanostructures. The inset shows the stability performance of as-synthesized MoS_2 nanosheet/TiO_2 nanowire hybrid structures as photo co-catalyst in visible light photocatalytic HER.

Conclusions

In summary, the MoS_2 nanosheet/porous TiO_2 nanowire hybrid nanostructures were successfully synthesized by a simple hydrothermal method, leading to an enhanced surface area. This 1D hybrid structures with the porous core as co-catalyst exhibit high activity in the visible-light photocatalytic hydrogen evolution reaction with an enhanced hydrogen generation rate of 16.7 mmol • h^{-1} • g^{-1}. This 1D hybrid nanostructure as co-catalyst provides us some general guidelines for overcoming the low efficiency of the other catalysts in water splitting reactions.

This work was supported by National Natural Science Foundation of China (NSFC) (21373196, 21271166), the Recruitment Program of Global Experts, the Fundamental Research Funds for the Central Universities (WK2060140014, WK2340000050).

Notes and references

[a] Department of Materials Science & Engineering, CAS key Laboratory of Materials for Energy Conversion, University of Science and Technology of China, Hefei, Anhui, 230026, China.
[b] Molecular Foundry, Lawrence Berkeley National Laboratory, 1 Cyclotron Rd, Berkeley, CA 94720, USA.
* binxiang@ustc.edu.cn; dupingwu@ustc.edu.cn

† Electronic Supplementary Information (ESI) available: Details of synthesis and characterization. See DOI: 10.1039/c000000x/

1 D. Voiry, M. Salehi, R. Silva, T. Fujita, M. Chen, T. Asefa, V. B. Shenoy, G. Eda and M. Chhowalla, *Nano Lett.*, 2012, **13**, 6222.
2 H. Hwang, H. Kim and J. Cho, *Nano Lett.*, 2011, **11**, 4826.
3 P. D. Fleischauer, J. R. Lince, P. A. Bertrand and R. Bauer, *Langmuir*, 1989, **5**, 1109.
4 H. S. Lee, S. W. Min, Y. G. Chang, M. K. Park, T. Nam, H. Kim, J. H. Kim, S. Ryu and S. Im, *Nano Lett.*, 2012, **12**, 3695.
5 O. Lopez-Sanchez, D. Lembke1, M. Kayci, A. Radenovic and A. Kis, *Nat. Nanotechnol.*, 2013, **8**, 497.
6 K. F. Mak, C. Lee, J. Hone, J. Shan and T. F. Heinz, *Phys. Rev. Lett.*, 2010, **105**, 136805.
7 C. Lee, H. Yan, L. E. Brus, T. F. Heinz, J. Hone and S. Ryu, *ACS Nano*, 2010, **4,** 2695.
8 X. Zong, H. Yan, G. Wu, G. Ma, F. Wen, L. Wang and C. Li, *J. Am. Chem. Soc.*, 2008, **130**, 7176.
9 K. Chang, Z. Mei, T. Wang, Q. Kang, S. Ouyang and J. Ye, *ACS Nano*, 2014, **8,** 7078
10 A. B. Laursen, S. Kegnæs, S. Dahla and Ib. Chorkendorff, *Energy Environ. Sci.*, 2012, **5**, 5577.
11 S. Kanda, T. Akita, M. Fujishima and H. Tada, *J. Colloid Interface Sci.*, 2011, **354,** 607.
12 X. Zong, Y. Na, F. Wen, G. Ma, J. Yang, D. Wang, Y. Ma, M. Wang, L. Sunbc and C. Li, *Chem. Commun.*, 2009, 4536.
13 B. Hinnemann, P. G. Moses, J. Bonde, K. P. Jørgensen, J. H. Nielsen, S. Horch, I. Chorkendorff and J. K. Nørskov, *J. Am. Chem. Soc.*, 2005, **127**, 5308.
14 T. F. Jaramillo, K. P. Jorgensen, J. Bonde, J. H. Nielsen, S. Horch and I. Chorkendorff, *Science*, 2007, **317**, 100.
15 J. Bonde, P. G. Moses, T. F. Jaramillo, J. K. Nørskovb and I. Chorkendorff, *Faraday Discuss.*, 2008, **140**, 219.
16 Q. Xiang, J. Yu and M. Jaroniec, *J. Am. Chem. Soc.*, 2012, **134**, 6575.
17 S. Min and G. Lu, *J. Phys. Chem. C,* 2012, 116, 25415.
18 W. Zhou, Z. Yin, Y. Du, X. Huang, Z. Zeng, Z. Fan, H. Liu, J. Wang and H. Zhang, *Small*, 2013, **9**, 140.
19 D. Li and Y. Xia, *Nano Lett.*, 2003, **3**, 555.
20 C. Y. Xu, P. X. Zhang and L. Yan, *J. Raman Spectrosc.*, 2001, **32**, 862.
21 L. Yang, X. Cui, J. Zhang, K. Wang, M. Shen, S. Zeng, S. A. Dayeh, L. Feng and B. Xiang, *Sci. Rep.*, 2014, DOI: 10.1038/srep05649.
22 R. Coehoorn and C. Haas, *Phys. Rev. B*, 1987, **35**, 6203.
23 V. Chikan and D. F. Kelley, *J. Phys. Chem. B*, 2002, **106**, 3794.